Influence of CTE Mismatch on Debonding and Particulate Damage in AA1100 Alloy/ZrC Nanoparticulate Metal Matrix Composites

Chennakesava R Alavala

Professor, Department of Mechanical Engineering, JNT University, Hyderabad, India

ABSTRACT: The aim of the present work was to predict the interface debonding and ZrC nanoparticulate fracture using RVE models through finite element analysis. The RVE model was designed from the square nanoparticulate distribution. The plane strain condition was assumed for 2-dimensional analysis of the composites. The major conclusion is that the ZrC nanoparticulates fracture above $100^{\circ}C$.

KEYWORDS: Zirconium carbide, AA1100 alloy, Particulate fracture, interface debonding, RVE model, finite element analysis.

I. INTRODUCTION

Nanoparticulate reinforced metal matrix composites are of great concern for several industrial applications due to their higher stiffness and strength than the alloys used for the matrix [1, 2]. Deep understanding of thermoplastic behaviour of the nanoparticulate reinforced metal matrix composites is an important subject in boosting up of those materials. The mismatch in coefficient of thermal expansion (CTE) and thermal conductivity between the nanoparticles and matrix can induce large stresses within the inclusions or at the matrix–nanoparticle interfaces. Several reinforcing materials nanoparticulates such as silicon carbide [3-7], alumina [8-10], boron carbide [11, 12], titanium boride [13, 14], silicon nitride [15-17], alumina trihydrate [18], carbon [19], etc were tested to improve the strength and stiffness.

The present work was to investigate the influence of CTE mismatch on interface debonding and particulate fracture in AA1100 alloy/ZrC nanoparticulate metal matrix composites. Finite element analysis (FEA) was executed using representative volume element (RVE) subjected to hydrostatic and isothermal loading.

II. MATERIAL AND METHODS

The shear lag model [20] has been used to describe the build up and transfer of particle stress, σ_p from the point where the particle enters the matrix to some point along the particle axis where the tensile stress has decayed to zero. Failure of the particle/matrix interface occurs when the interfacial shear strength, τmax, is reached.

The shear lag distribution of strain, along a fully bonded particle can be described by [20]

$$e_{app} = e_p \frac{sibh[n(L_{e-x/r})]}{sinH(ns)} \tag{1}$$

where e_{app} is the strain acting on the particle outside the matrix, e_p is the particle strain at a distance x inside the matrix, Le is the embedded length, r is the particle radius and s is the particle aspect ratio (L_e/r). The n parameter used in this paper is based on the parameter [14-16]:

$$n^2 = \frac{2}{E_p E_m}\left[\frac{E_p V_p + E_m V_m}{V_m/(4G_p) + 1/(2G_m)\left((1/V_m)\ln(1/V_p) - 1 - (V_m/2)\right)}\right] \tag{2}$$

where E_p and G_P ate the particle elastic and shear moduli, E_m and G_m are the elastic and shear moduli of the matrix. V_p is the particle volume fraction and V_m is the volume fraction of matrix. The corresponding interfacial stress, τ at a distance x along the interface, is given by

$$\tau = \frac{n}{2}E_p e_{app} \frac{\cosh[n(L_e-x)/r]}{\sinh[ns]} \tag{3}$$

Is a maximum at the crack plane (x = 0). Since both the interfacial shear stress and the stress acting on the particle, are a maximum at the crack-plane then failure should be expected to initiate from this point. When x = 0, the Eq. (3) becomes:

$$\tau = \frac{n}{2}E_p e_p \tag{4}$$

If the particle deforms in an elastic manner (according to Hooke's law) then,

$$\tau = \frac{n}{2}\sigma_p \tag{5}$$

where σ_p is the particle stress. If particle fracture occurs when the stress in the particle reaches its ultimate tensile strength, $\sigma_{p,uts}$, then setting the boundary condition at

$$\sigma_p = \sigma_{p,uts} \tag{6}$$

and substituting into Eq.(5) gives a relationship between the strength of the particle and the interfacial shear stress such that if

$$\sigma_{P,uts} < \frac{2\tau}{n} \tag{7}$$

Then the particle will fracture. Similarly if interfacial debonding/yielding is considered to occur when the interfacial shear stress reaches its shear strength

$$\tau = \tau max \tag{8}$$

Then by substituting Eq. (8) into Eq.(5) a boundary condition for particle/matrix interfacial fracture can be established whereby,

$$\tau_{max} < \frac{n\sigma_p}{2} \tag{9}$$

This approach suggests that the outcome of a matrix crack impinging on an embedded particle depends on the balance between the particle strength and the shear strength of the interface.

A linear stress–strain relation [15-18] at the macro level can be formulated as follows:

$$\bar{\sigma} = \bar{C}\bar{\varepsilon} \tag{10}$$

where $\bar{\sigma}$ is macro stress, and $\bar{\varepsilon}$ represents macro total strain and $\bar{C}$ and is macro stiffness matrix.

For plane strain conditions, the macro stress- macro strain relation [13, 14] is as follows:

$$\begin{Bmatrix} \overline{\sigma_x} \\ \overline{\sigma_y} \\ \overline{\tau_{xy}} \end{Bmatrix} = \begin{bmatrix} \overline{C_{11}} & \overline{C_{12}} & 0 \\ \overline{C_{21}} & \overline{C_{22}} & 0 \\ 0 & 0 & \overline{C_{33}} \end{bmatrix} \times \begin{Bmatrix} \overline{\varepsilon_x} \\ \overline{\varepsilon_y} \\ \overline{\gamma_{xy}} \end{Bmatrix} \tag{11}$$

The interfacial tractions can be obtained by transforming the micro stresses at the interface as given in Eq. (3):

$$t = \begin{Bmatrix} t_z \\ t_n \\ t_t \end{Bmatrix} = T\sigma \tag{12}$$

$$\text{where, } T = \begin{bmatrix} 0 & 0 & 0 \\ \cos^2\theta & \sin^2\theta & 2\sin\theta\cos\theta \\ -\sin\theta\cos\theta & \sin\theta\cos\theta & \cos^2\theta - \sin^2\theta \end{bmatrix}$$

AA1100 alloy was used as the matrix material. The filler material was ZrC of average size 100nm. The material properties are given in table 1. The volume fractions of ZrC nanoparticles were 10% and 30%. A square RVE (Fig. 1) was modeled to compute the thermoelastic behavior AA1100 alloy/ZrC nanocomposites. The PLANE183 element was used to discretize the matrix and nanoparticle. The interphase between the nanoparticle and matrix was discretized with CONTACT172 element [21]. Both isothermal and hydrostatic pressure loads were applied at simultaneously on the RVE models.

International Journal of Innovative Research in Science, Engineering and Technology

(An ISO 3297: 2007 Certified Organization)

Vol. 5, Issue 3, March 2016

Table 1: Mechanical properties of AA1100 matrix and ZrC nanoparticles

Property	AA1100	ZrC
Density, g/cc	2.71	6.73
Elastic modulus, GPa	68.9	430
Ultimate tensile strength, MPa	110	874
Poisson's ratio	0.33	0.25
CTE, μm/m-^{o}C	21.8	6.8
Thermal Conductivity, W/m-K	220.0	25
Specific heat, J/kg-K	904	368
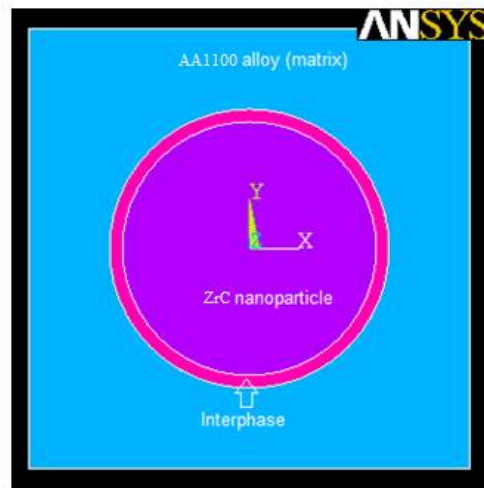
Fig.1. The RVE model.

III. **RESULTS AND DISCUSSION**

The influence of CTE on interface debonding and particulate fracture was assessed in terms of stress-strain relations, interfacial normal and tangential tractions and elastic modulus.
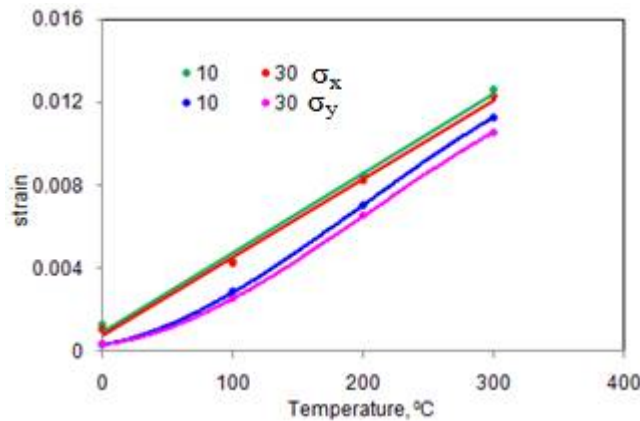

Fig. 2. Influence of temperature on thermoelastic strain.

A. *Micromechanics of thermo-elastic behaviour*

As the temperature increased, the strains become much larger than the experimental data because the softening occurs in the nanocomposites (Fig. 2). Due to high ductility and thermal expansion of AA1100 alloy matrix, the strains developed in it were higher than those of ZrC nanoparticles (Fig. 3).
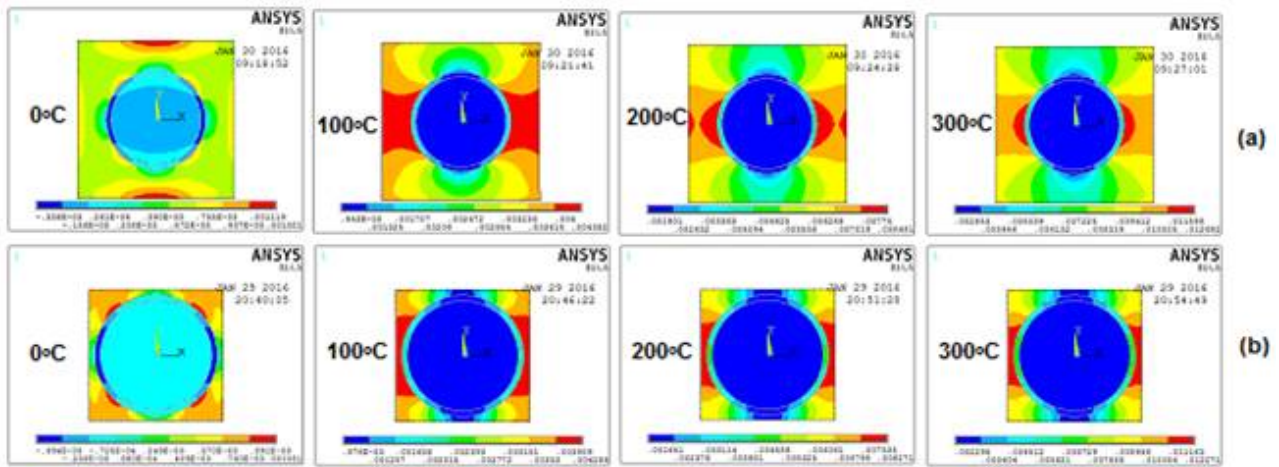

Fig.3. Raster images of tensile strains induced in (a) AA1100/10%ZrC and (b) AA1100/30% ZrC composites.

The stresses induced in the composites increased with the increase of temperature as shown in Fig. 4. The stresses are higher along the tensile load direction than those developed along the transverse direction of loading. This reveals a progressive shift from local plastic flow to bulk flow of matrix material because of temperature instigated softening.
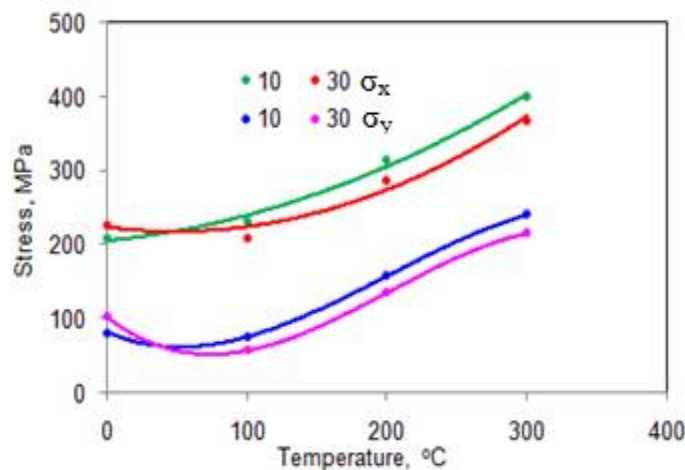

Fig. 4. Influence of temperature on strength.

Fig 5 shows tensile stresses obtained by the finite element analysis in the composites having 10% and 30% ZrC nanoparticles. The stress was very high either in ZrC nanoparticles or at the interphase on account of load transfer from the matrix to the nanoparticle. The elastic moduli (E_x and E_y) and major Poisons ratio (v_{12}) were evaluated for volume fractions from 10% and 30%. The tensile elastic modulus decreased with the increase of temperature (Fig. 6a). The major Poisson's ratio increased with increase of temperature (Fig. 6b).
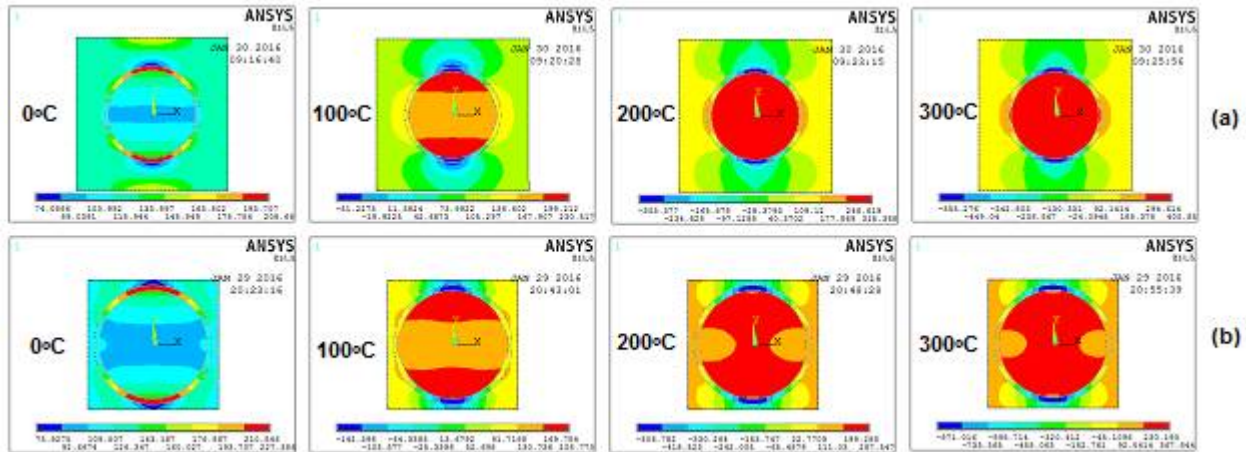
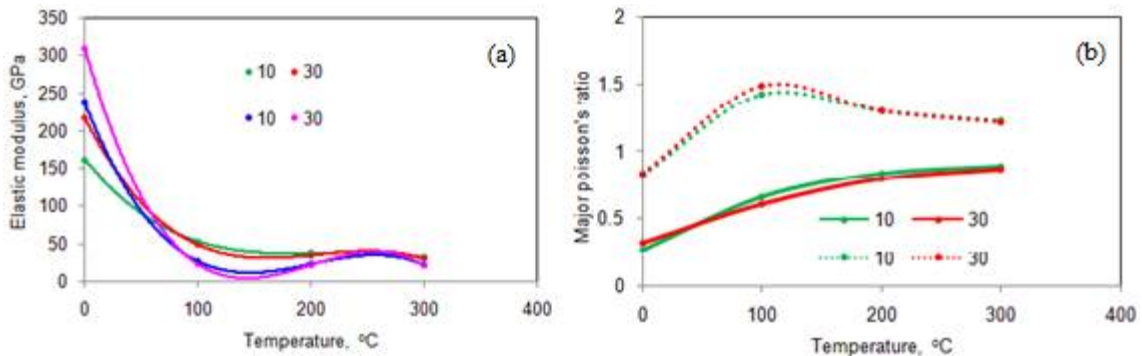Fig. 5. Raster images of tensile stresses induced in AA1100/10% ZrC and (b) AA1100/30% ZrC composites.

Fig. 5. Influence of temperature on (a) Ex, (b) Ey and (c) major Poisson's ratio.

B. *Debonding and particle fracture*

Influence of temperature on failure criteria in the composites is shown in Fig. 6. It is observed that the particulate fracture has occurred above $100^{o}C$ as the condition $\sigma_p < 2\tau/n$ is satisfied (Fig. 6a) for the composites having 10%ZrC particulates while it is above $75^{o}C$ for the composites comprising 30%ZrC particulates. The debonding of interface/interphase has occurred below $100^{o}C$ (Fig. 6b).
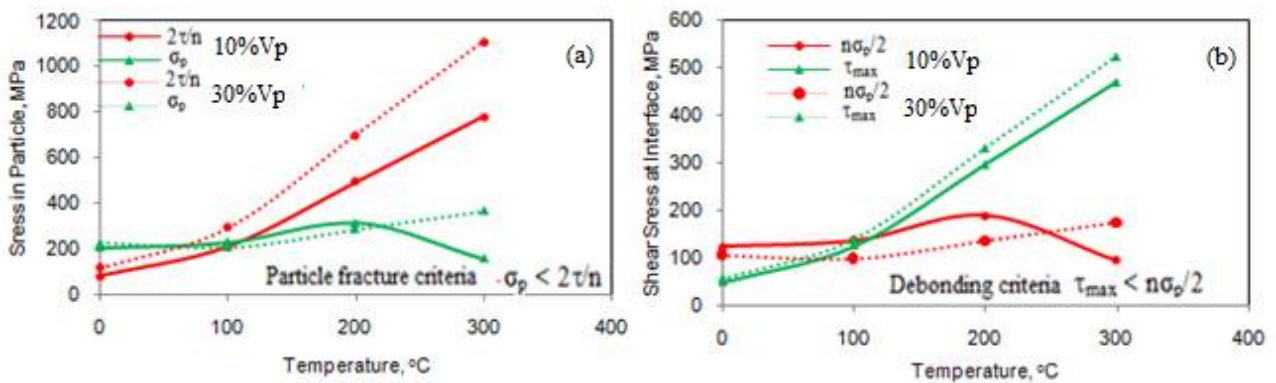

Fig. 6. Failure criteria: (a) Particulate fracture and (b) interface debonding.

The scanning electron microscope (SEM) image (Fig. 7) demonstrates the interface rupture in the composites having 30%ZrC at 100°C. Tear bands are also seen in the ZrC nanoparticulate due to CTE mismatch between the ZrC particulate and AA1100 alloy matrix.
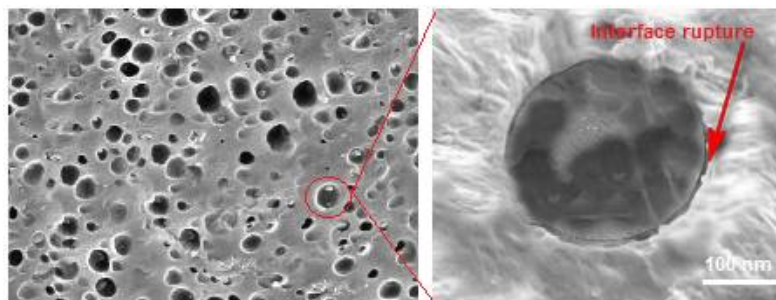

Fig. 7. SEM images illustrating rupture of interphase and tear bands in nanoparticles at 100°C.

IV. CONCLUSIONS

The fracture of ZrC nanoparticulate is highly dependent on the temperature. The debonding of interface has occurred below 100°C and ZrC particulate fracture has resulted above 100°C. The likelihood of particulate fracture was high in the composites having 30%Vp of ZrC. The stiffness of ZrC/AA1100 alloy metal matrix composites decreased with the increase of temperature.

REFERENCES

[1] Reddy, A. C., Kotiveerchari, B. Rami Reddy, P. "Saving of Thermal Energy in Air-Gap Insulated Pistons Using Different Composite Materials for Crowns," International Journal of Scientific & Engineering Research, vol. 6, no. 3, pp. 71-74, 2015.
[2] Chawla, K. K. "Composite Materials: Science and Engineering," Springer-Verlag, 1998.
[3] Reddy, A. C. "Tensile properties and fracture behavior of 6063/SiCP metal matrix composites fabricated by investment casting process," International Journal of Mechanical Engineering and Materials Sciences, vol.3, no.1, pp.73-78, 2010.
[4] Reddy, A. C. "Experimental Evaluation of Elastic Lattice Strains in the Discontinuously SiC Reinforced Al-alloy Composites," National Conference on Emerging Trends in Mechanical Engineering, Nagapur, 05-06th February, 2004.
[5] Reddy, A. C. "Influence of strain rate and temperature on superplastic behavior of sinter forged Al6061/SiC metal matrix composites," International Journal of Engineering Research & Technology, vol.4, no.2, pp.189-198, 2011.
[6] Reddy, A. C., Kotiveerachari, B. "Influence of microstructural changes caused by ageing on wear behaviour of Al6061/SiC composites," Journal of Metallurgy & Materials Science, vol. 53, no. 1, pp. 31-39, 2011.
[7] Geni, M., Kikuchi, M. "Damage Analysis of Aluminum Matrix Composite Considering Non-uniform Distribution of SiC Particles," Acta Metallurgica, vol.46, no.9, pp.3125-3133, 1998.
[8] Reddy, A. C. "Strengthening mechanisms and fracture behavior of 7072Al/Al2O3 metal matrix composites," International Journal of Engineering Science and Technology, vol.3, no.7, pp.6090-6100, 2011.
[9] Reddy, A. C., Essa Zitoun, Matrix al-alloys for alumina particle reinforced metal matrix composites, Indian Foundry Journal, vol.55, no.01, pp.12-16, 2009.
[10] Pestes, R. H., Kamat, S.V., Hirth, J.P. "Fracture toughness of Al-4%Mg/Al$_2$O$_3$ composites," Materials Science & Engineering, A: Structural Materials: Properties, Microstructure and Processing, vol.189A, pp. 9-14, 1994.
[11] Reddy, A. C. "Effect of Particle Loading on Microealstic Behavior and interfacial Tractions of Boron Carbide/AA4015 Alloy Metal Matrix Composites," 1st International Conference on Composite Materials and Characterization, Bangalore, 14-15 march 1997.
[12] Cun, Z. N., Jia, J. G., Jun, L. L., Zhang, D. "Production of Boron Carbide Reinforced 2024 Aluminum Matrix Composites by Mechanical Alloying," Materials Transactions, vol. 48, no. 5, pp. 990 to 995, 2007.
[13] Reddy, A. C. "Interfacial Debonding Analysis in Terms of Interfacial Tractions for Titanium Boride/AA3003 Alloy Metal Matrix Composites," 1st National Conference on Modern Materials and Manufacturing, Pune, 19-20 December 1997.
[14] Reddy, A. C. "Reckoning of Micro-stresses and interfacial Tractions in Titanium Boride/AA2024 Alloy Metal Matrix Composites," 1st International Conference on Composite Materials and Characterization, Bangalore, 14-15 march 1997.

[15] Reddy, A. C. "Evaluation of Debonding and Dislocation Occurrences in Rhombus Silicon Nitride Particulate/AA4015 Alloy Metal Matrix Composites," National Conference on Materials and Manufacturing Processes, Hyderabad, 27-28 February 1998.

[16] Reddy, A. C. "Assessment of Debonding and Particulate Fracture Occurrences in Circular Silicon Nitride Particulate/AA5050 Alloy Metal Matrix Composites," National Conference on Materials and Manufacturing Processes, Hyderabad, 27-28 February 1998.

[17] Reddy, A. C. "Evaluation of Debonding and Dislocation Occurrences in Rhombus Silicon Nitride Particulate/AA4015 Alloy Metal Matrix Composites," 1st National Conference on Modern Materials and Manufacturing, Pune, 19-20 December 1997.

[18] Reddy, A. C. "Studies on fracture behavior of brittle matrix and alumina trihydrate particulate composites," Indian Journal of Engineering & Materials Sciences, vol.9, No.5, pp.365-368, 2002.

[19] Reddy, A. C. "Analysis of the Relationship Between the Interface Structure and the Strength of Carbon-Aluminum Composites," NATCON-ME, Bangalore, 13-14th March 2004.

[20] Suresh, S., Mortensen, A., Needleman, A. "Fundamentals of MMCs," Butterworth- Heinemann Publishing Company, Stoneham, USA, 1993.

[21] Alavala, C.R. "Finite Element methods: Basic Concepts and Applications," PHI Learning Pvt. Ltd., New Delhi, 2008.